Simultaneous Nano- and Microscale Control of Nanofibrous Microspheres Self-Assembled from Star-Shaped Polymers

*Zhanpeng Zhang, Ryan L. Marson, Zhishen Ge, Sharon C. Glotzer, and Peter X. Ma**

Spherical micro- and nanostructured particles are important elements of many current and future technologies, including delivery of chemical and biological molecules,[1] fabrication of electronic displays,[2] preparation of photonic,[3] plasmonic,[4] and photosynthetic[5] assemblies and self-healing structural materials,[6] as well as separation, sensing, and catalysis.[7] The external and internal structures of the microsphere are critical to their function and performance. For tissue regeneration, a porous structure on the micrometer scale can increase cell-loading efficiency, improve nutrition transport, decrease the amount of degradation products, and facilitate vascularization and tissue formation.[8] On the nanometer scale, a nanofibrous structure mimics the structure of collagen and improves cell–matrix interactions.[9] Recently, unusual nanofibrous, hollow microspheres were synthesized from star-shaped poly(L-lactic acid) (SS-PLLA), which integrated both a fibrous nanostructure and a hollow microstructure for the first time.[10] However, the underlying mechanism of the nanofibrous hollow microsphere formation was unclear. In this study, we demonstrate via experiments and computer simulations how the molecular structure of SS-PLLA dictates its self-assembly on both the nano- and micrometer scales, and we describe a versatile method to prepare microspheres with simultaneously controlled nano- and microstructures.

Dr. Z. Zhang, Prof. P. X. Ma
Department of Biomedical Engineering
University of Michigan
Ann Arbor, MI 48109-1078, USA
E-mail: mapx@umich.edu
Dr. R. L. Marson, Prof. S. C. Glotzer, Prof. P. X. Ma
Materials Science and Engineering
University of Michigan
Ann Arbor, MI 48109-1078, USA
Dr. R. L. Marson, Prof. S. C. Glotzer, Prof. P. X. Ma
Biointerfaces Institute
University of Michigan
Ann Arbor, MI 48109-1078, USA
Dr. Z. Ge, Prof. P. X. Ma
Department of Biologic and Materials Sciences
University of Michigan
Ann Arbor, MI 48109-1078, USA
Prof. S. C. Glotzer
Department of Chemical Engineering
University of Michigan
Ann Arbor, MI 48109-1078, USA
Prof. S. C. Glotzer, Prof. P. X. Ma
Macromolecular Science and Engineering Center
University of Michigan
Ann Arbor, MI 48109-1078, USA

DOI: 10.1002/adma.201501329

To study how the molecular architecture of star-shaped polymers affects assembly, we choose initiators with X initiating sites (hydroxyls (OH)) to polymerize L-lactide (LLA) to generate SS-PLLA with q arms (X = 2, 3, 4, 8, 16, 32, and 64, Figure S1, Supporting Information). The theoretical arm length is calculated from the feeding ratio, LLA:OH (= Y). The actual average arm length N is determined by ^{1}H-NMR. It should be noted that the $q < X$ and $N > Y$ when $X \geq 8$ because not all hydroxyls participate in the polymerization due to steric hindrance.[11] The polymers are abbreviated as X-arm PLLA-Y (Table S1, Supporting Information). Emulsification and thermally induced phase separation (TIPS) techniques are used to fabricate the microspheres from these SS-PLLAs (**Figure 1**A). Specifically, glycerol is gradually added (Figure 1A(a,b)) into a 2% (w/v) SS-PLLA/tetrahydrofuran (THF) solution (glycerol:SS-PLLA/THF = 3:1 (v/v)), which causes phase inversion and three types of emulsions to form (Figure 1A(c–e)). The emulsions are then quenched in liquid nitrogen to induce nanometer scale phase separation of the polymer solution (Figure 1A(f)). After glycerol and THF extraction with distilled ice water, the microspheres (Figure 1A(g–i)) are freeze-dried and stored in vacuum.

Quenching the emulsions in liquid nitrogen induces nanoscale phase separation of the polymer solution (Figure 1A(f)). During this thermodynamic process, polymer solutions undergo separation into bicontinuous nanoscale phases (presumably through a spinodal decomposition pathway), SS-PLLA chains rearrange to maximize formation of crystalline domains, and ultimately nanofibers form.[12,13] According to the Flory–Huggins (FH) theory, the FH polymer–solvent interaction parameter, χ, must exceed a critical value χ_c to trigger the spinodal decomposition pathway.[14] Increasing the molecular weight (M_w) of a polymer can reduce χ_c to trigger the spinodal decomposition. In addition to the initiation of the spinodal phase separation, the stabilization of the phase-separated nanofibrous patterns is needed to obtain nanofibers. It is known that crystallinity of SS-PLLA increases as arm length increases.[15] Therefore, sufficiently long arm length is also needed to crystallize the nanofibers (Table S2, Supporting Information). Here, we find that SS-PLLAs assemble into nanofibers only when the arm length N is above a critical value (denoted as N_c) (Figure 1B,C). $N_c \approx 200$ when X = 2, 3, 4; $N_c \approx 150$ when X = 8, 16, 32; and $N_c \approx 200$ when X = 64 (Table S1, Supporting Information). Therefore, an approximate universal N_c (including linear PLLA (with two arms) and

ADVANCED MATERIALS
www.advmat.de

www.MaterialsViews.com

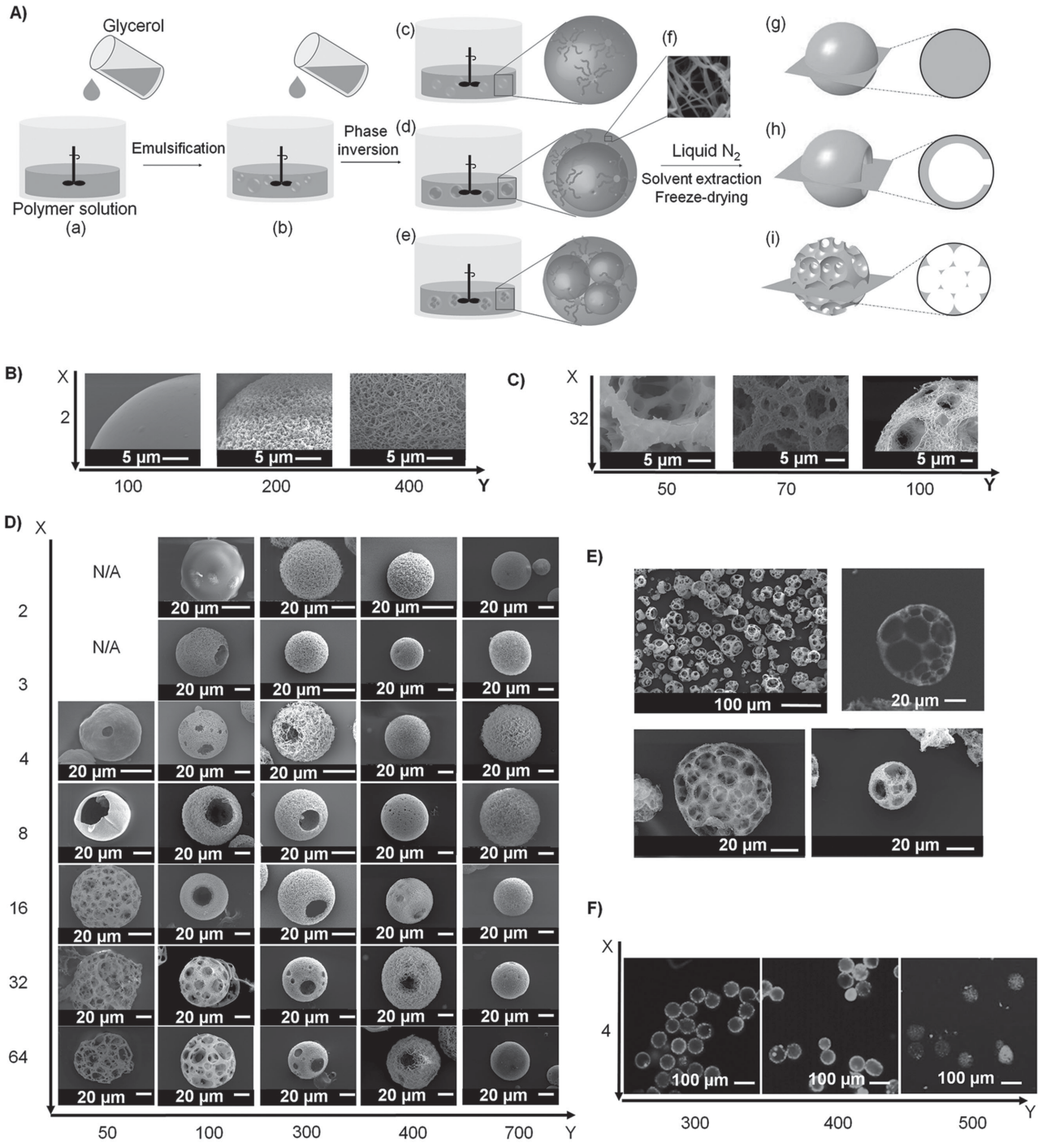

Figure 1. A) An illustration of the combination of emulsification and thermally induced phase separation to fabricate nano- and microstructured spheres. a,b) Glycerol is slowly poured into a stirred polymer solution. c–e) As the amount of the added glycerol increases, catastrophic phase inversion occurs, generating three types of emulsions: c) a single emulsion (simple polymer droplets); d) a double emulsion (one inner droplet of glycerol inside one polymer droplet); and e) an emulsion with multiple inner droplets of glycerol inside one polymer droplet (referred as "multiple emulsion" hereafter). f) Emulsions are quenched in liquid nitrogen to induce phase separation on the nanometer scale. Upon solvent/glycerol extraction and freeze-drying, g) the single emulsions form nonhollow microspheres; h) the double emulsions form hollow microspheres; and i) the multiple emulsions form spongy microspheres. B–F) Structural characterization of microspheres fabricated from SS-PLLA of different *X* and *Y*. B–D) SEM images of microspheres fabricated from B) two-arm PLLAs with *Y* = 100, 200, and 400. Scale bars: 5 μm; C) 32-arm PLLAs with Y = 50, 70, and 100. Scale bars: 5 μm; D) SS-PLLAs of different *X* and *Y*, showing the structural transition process as *X* and *Y* changes. Scale bars: 20 μm. E) SEM and cross-sectional confocal images of microspheres formed from 32-arm PLLA-100. Scale bars: 100 μm in top left panel and 20 μm in the rest of the panels; F) Cross-sectional confocal images of microspheres fabricated from four-arm PLLAs with *Y* = 300, 400, and 500. Scale bars: 100 μm.

all the examined SS-PLLAs) appears in the range of 150–200. When $N > N_c$, any SS-PLLA forms nanofibers. Decreasing N leads to fiber aggregation (Figure 1B (middle) and Figure 1C (middle)), and ultimately a smooth (dense) microsphere formation (Figure 1B(left) and Figure 1C(left)).

Prior to nanometer scale phase separation, SS-PLLAs phase separate on the microscale during emulsification. Three types of microstructures are identified: nonhollow microspheres (Figure 1A(g)), hollow microspheres with one or multiple pore openings on the shell (Figure 1A(h)), and spongy microspheres with an interconnected pore structure (Figure 1A(i)). This suggests that single emulsions, double emulsions, and multiple emulsions are formed, respectively (Figure 1A(c–e)). It should be noted that the hole on the surface of hollow microspheres is caused by the phase inversion process, which connects the encapsulated glycerol and the outer glycerol phase.[10] Combined with the two types of observed nanoscale structure (smooth and nanofibrous), six distinct types of microspheres are formed: smooth nonhollow microspheres, nanofibrous nonhollow microspheres, smooth hollow microspheres, nanofibrous hollow microspheres, smooth spongy microspheres, and nanofibrous spongy microspheres (Figure 1D). The characterization of the spheres (porosity, surface area, overall density) is summarized in Table S2 (Supporting Information). Of particular note is the nanofibrous spongy microsphere, which integrates a nanofibrous structure with an internally interconnected multipore structure into microspheres with an increasing number of pores as the diameter increases (Figure 1E).

The values of both X and Y affect the microstructure of the spheres. On the one hand, a small Y favors a more porous microstructure. For example, 16-arm PLLAs transition from nonhollow microspheres to hollow microspheres to spongy microspheres when Y decreases from 700 to 50. Four-arm PLLAs transition from hollow to nonhollow microspheres when Y increases from 300 to 500 (Figure 1F). On the other hand, when Y is fixed, an increased X produces a more porous structure. For instance, when $Y = 100$, microspheres transition from nonhollow to hollow to spongy as X increases from 2 to 64. We speculate that the hydroxyls of the SS-PLLAs (located at the end of each arm, as well as in the unreacted sites of the initiator core) are responsible for the hollow/spongy structure formation, because the change of the molecular architecture affects the hydroxyl density of the polymers. Here, the hydroxyl density of SS-PLLA, denoted as **OH/LLA**, is calculated from the molar ratio of hydroxyls to monomer LLA. Thus, **OH/LLA** = $1/Y$. We therefore hypothesize that: i) the hydroxyl groups are required for the hollow/spongy structure formation, and ii) a high **OH/LLA** value favors the formation of a hollow/spongy structure. Two experiments are designed to test these hypotheses. In the first experiment, we cap the hydroxyls of SS-PLLA prior to emulsification and TIPS (Figure S2a, Supporting Information). The hydroxyl-capping reaction "turns off" the polymer's ability to self-assemble into hollow microspheres. For example, four-arm PLLA100, which is capable of forming hollow microspheres (Figure 1D), assembles into nonhollow microspheres after the hydroxyl capping reaction (**Figure 2**a). This finding supports our first hypothesis that the hydroxyl groups on SS-PLLA are required for the hollow structure formation. In the second experiment, we double **OH/LLA** without altering X or Y (Figure S2b, Supporting Information). Four-arm PLLA-400, which has a low **OH/LLA** value (1/400) and forms nonhollow microspheres (Figure 1D), assembles into hollow microspheres after its **OH/LLA** is increased to 1/200 (Figure 2b). 16-arm PLLA-100 (**OH/LLA** = 1/100), which forms hollow microspheres (Figure 1D) before modification, assembles into spongy microspheres after hydroxyl doubling (**OH/LLA** increased to 1/50) (Figure 2c). These findings support our second hypothesis that a higher **OH/LLA** favors hollow/spongy structure formation. In these two experiments, the modification does not alter the nanometer scale phase separation, which agrees with our previous discussion that the nanometer scale phase separation is mainly a result of polymer chain–solvent interaction (arm length). Associating the hollow/spongy structure formation with the **OH/LLA** of the SS-PLLAs, we determine the **OH/LLA** threshold values for structural transition of the spheres on the microscale (Table S3, Supporting Information). Figure 2d shows a phase diagram summarizing the nano- and microscale self-assembly as a function of X and Y.

We further hypothesize that the hydroxyl groups of SS-PLLA stabilize the polymer solution/glycerol interface due to the high affinity of hydroxyl to glycerol. As a result, SS-PLLA with a higher **OH/LLA** favors the formation of double/multiple emulsions, which contain larger interfacial area than single emulsions. To test this hypothesis, we perform dissipative particle dynamics (DPD) simulations for 4-, 8-, and 16-arm polymers and for a range of arm lengths using HOOMD-Blue (http://codeblue.umich.edu/hoomd-blue).[16–18] For each set of arms, simulations are run for arm lengths of N_{bead} = 10, 40, 80, and 120 coarse grained beads, linked together with harmonic springs. To capture the catastrophic phase inversion process that causes the initial encapsulation of glycerol into the polymer solution droplets (Figure S3, Supporting Information), star polymers are initialized within a thin spherical shell. For simplicity, the encapsulated glycerol is not connected to the outer glycerol phase in this simulation study. Each simulation containing between 1.1 and 1.5 million particles is run for at least five million time steps to ensure proper equilibration, and additionally verified by running to 50 million time steps for one of each type of microspheres (nonhollow, hollow, and spongy). Larger simulations (containing ≈11 million particles, Figure S4, Supporting Information) of each type of microsphere are also run to rule out finite size or other nonphysical effects. In total, over 100 independent state points are simulated (full details in the simulation section of the Supporting Information).

For all simulated state points, a transition from hollow to nonhollow is observed as N_{bead} increases, supporting the experimental data. For star-shaped polymers with long arms, the polymer shell ruptures during the simulation and the glycerol mostly leaves the droplet, with only small pockets of solvent remaining inside (**Figure 3**a,b). For star-shaped polymers with short arms, the double emulsion droplet is stabilized, with the hydroxyl groups concentrated at both the interior and exterior interfaces (Figure 3c,d and Figure S4a,b, Supporting Information). By looking at a single star-shaped polymer molecule (Figure 3c), we find that the polymer "stretches" its arms to reach to the interfaces, acting like a surfactant capable of stabilizing both the interior and exterior interfaces. Increasing the strength of attraction between the hydroxyls and glycerol (mimicking the "hydroxyl doubling" modification experiment)

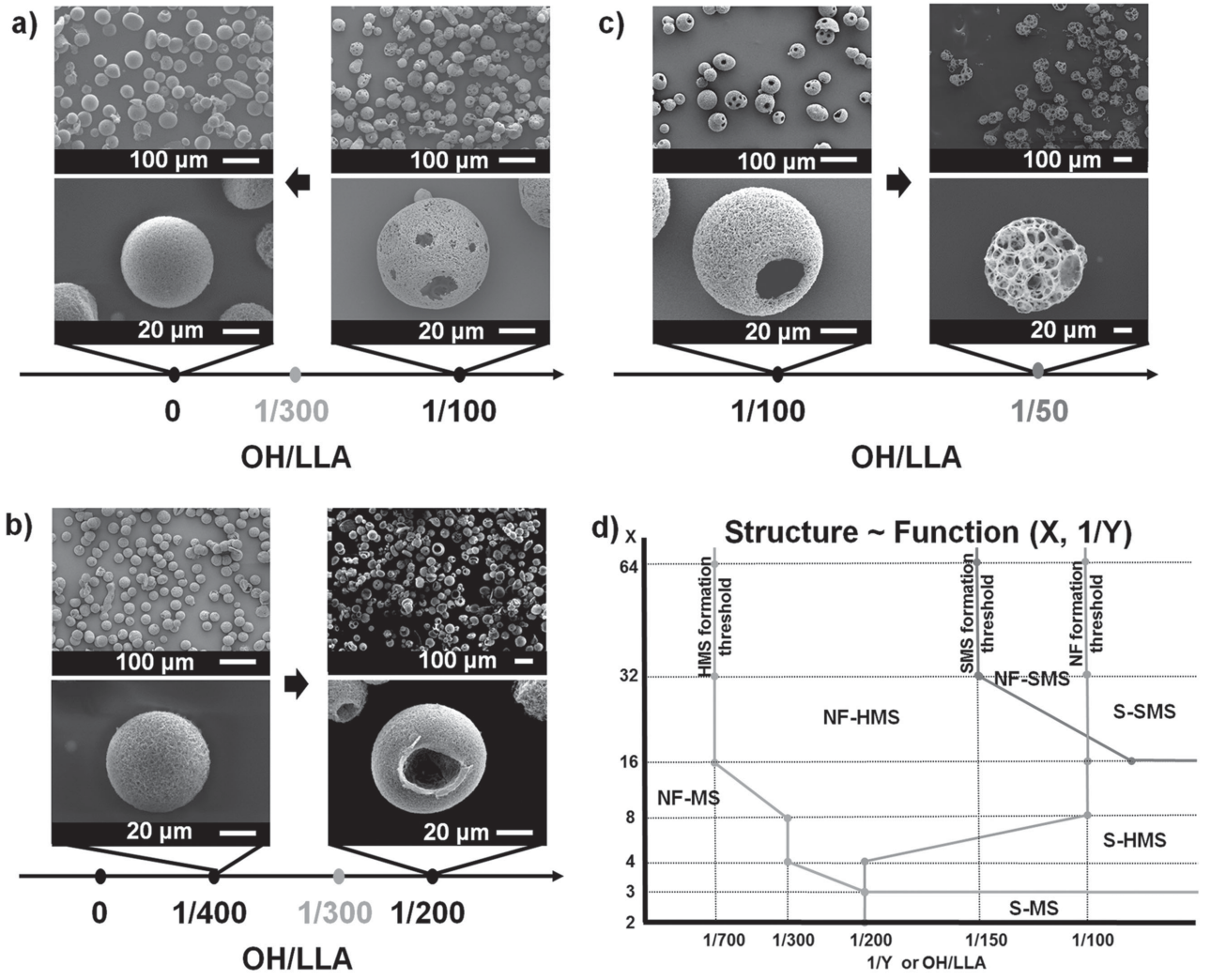

Figure 2. Hydroxyl density of SS-PLLA affects the microscale structure of microspheres. a–c) SEM images of microspheres fabricated from a) four-arm PLLA-100 before (right column) and after (left column) hydroxyl capping. b) Four-arm PLLA-200 before (left column) and after (right column) hydroxyl doubling. c) 16-arm PLLA-100 before (left column) and after (right column) hydroxyl doubling. The hollow-to-nonhollow transition point is 1/300 for four-arm PLLAs. The hollow-to-spongy transition point for 16-arm PLLAs is 1/50. Scale bars: 100 μm on the top row, 20 μm on the bottom row. d) The structure of microspheres as a function of arm number and arm length. Note: This graph is based on SS-PLLAs without modification. S-MS refers to smooth nonhollow microspheres, NF-MS refers to nanofibrous nonhollow microspheres, S-HMS refers to smooth hollow microspheres, NF-HMS refers to nanofibrous hollow microspheres, S-SMS refers to smooth spongy microspheres, NF-SMS refers to nanofibrous spongy microspheres. As 1/*Y* and *X* increase, the line that represents the boundary of the transition from MS to HMS is on the MS side, while the line that represents the boundary of the transition from HMS to SMS is on the SMS side. As 1/*Y* decreases and *X* increases, the line that represents the boundary of the transition from S to NF is on the NF side.

causes a transition from nonhollow to hollow structures, again matching the experimental data (Figure 2b). These results support our hypothesis that hydroxyls can stabilize the interior and exterior interfaces for hollow sphere formation. The high affinity between hydroxyls and glycerol probably stems from their hydrophilic interaction (e.g., hydrogen bonding), which lowers the interfacial tension and stabilizes the interfaces. In addition, for 16-arm polymers with N_{bead} = 10, glycerol molecules in the interior of the polymer solution droplet separate into multiple domains (Figure 3e,f and Figure S4c–f, Supporting Information), consistent with the experimental finding that 16-arm PLLA with short arms form spongy microspheres (Figure 1D). These simulation results indicate that, while the catastrophic phase inversion might initially cause the encapsulation of glycerol inside the polymer solution droplet (Figure 1A(b)), the final microstructure of the emulsions is determined by **OH/LLA** and the molecular structure of SS-PLLAs.

In summary, star-shaped polymers with varying arm numbers and arm lengths are synthesized, characterized, and simulated for the systematic study of their self-assembly during emulsification and TIPS processes. During these processes, phase separation on the nanometer and micrometer scales determines the final structure of the microspheres at these two levels. The nanoscale phase separation of SS-PLLA depends on arm length, while the microscale structure is determined by arm number and **OH/LLA** ratio. The discovered mechanisms

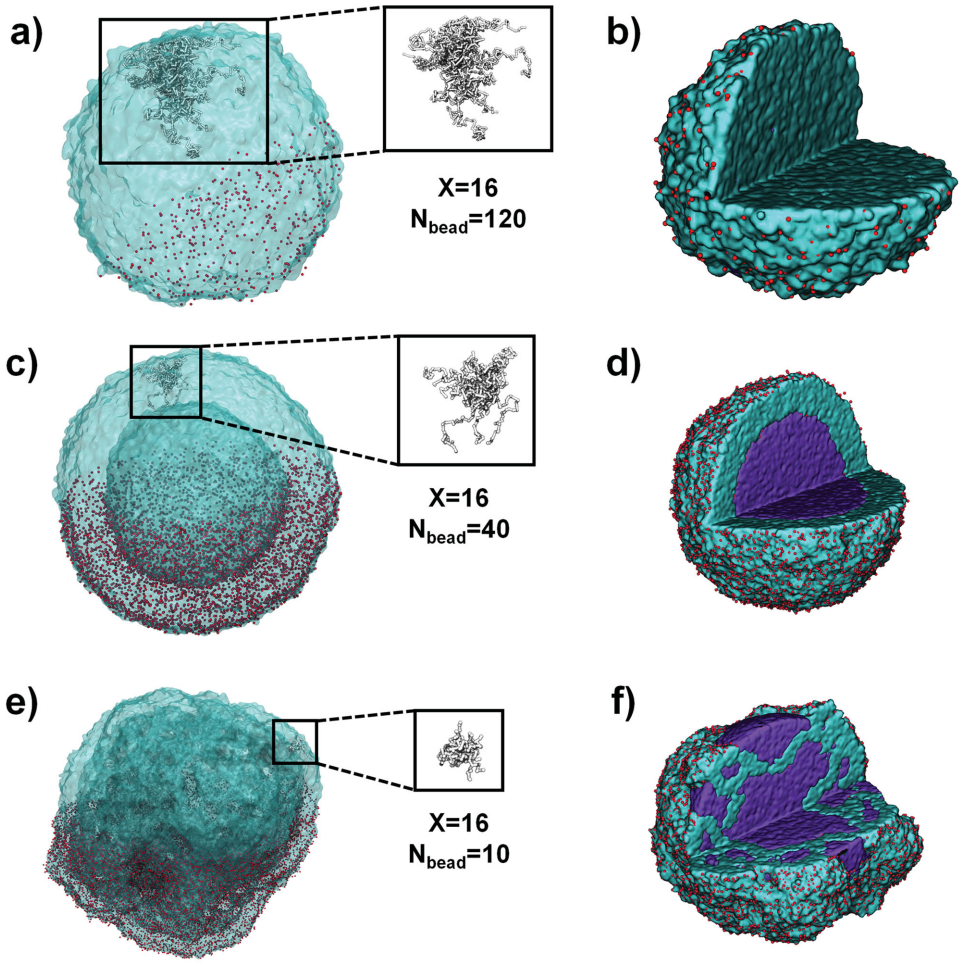

Figure 3. DPD simulations of 16-arm star-shaped polymers of varying arm lengths and the formation of different emulsions. For 16-arm PLLAs, as the length of the polymer arm decreases from 120 to 10, the structures undergo a transition from a,b) nonhollow (N_{bead} = 120) to c,d) hollow (N_{bead} = 40) to e,f) spongy (N_{bead} = 10). This occurs for a variety of polymer droplet concentrations and in other star polymer systems with different arm numbers. The left column of images (a,c,e) shows the polymer isosurface, with individual hydroxyl beads on the bottom half of the droplet shown in red. The conformation of a single 16-arm PLLA is shown in the square box. The right column (b,f,j) shows the internal structure of the same droplet in the left, with glycerol in purple. Some hydroxyls (red beads) are removed for clarity.

provide guidance on simultaneous control of nano- and microstructure formation and result in several novel microspheres, which may broadly impact biomedical and other emerging technologies. For example, the interconnected internal pore structure of spongy microspheres may enable deliberate control of cell–cell interactions to maximize regeneration outcome. The nano- and microstructured spheres may also provide advanced 3D substrates for catalysis or biosensing technologies.

Experimental Section

Synthesis of Star-Shaped PLLA: Star-shaped PLLA was prepared via ring-opening polymerization (ROP) of L-lactide. A detailed synthesis procedure can be found in the Supporting Information. Glycerol, pentaerythritol, *N*,*N*,*N*′,*N*′-tetra(2,3-dihydroxpropyl)ethane-1,2-diamine, PAMAM dendrimers (G2-OH, G3-OH, or G4-OH) were used as the initiators to generate linear PLLA, three-arm PLLA, four-arm PLLA, eight-arm PLLA, 16-arm PLLA, 32-arm PLLA, and 64-arm PLLA, respectively. The procedure for capping/doubling of hydroxyl groups are detailed in the Supporting Information.

Fabrication of Microspheres: The polymer (0.4 g) was dissolved in THF at 50 °C with a concentration of 2% w/v. Under rigorous mechanical stirring (Speed 9, Fisher Science Inc.), glycerol (50 °C) with three times the volume of star-shaped PLLA solution was gradually added into the polymer solution. After stirring for 5 min, the mixture was quickly poured into liquid nitrogen. After 10 min, water-ice mixture (1 L) was added for solvent exchange for 24 h. The microspheres were sieved and washed with distilled water eight times to remove residual glycerol on the sphere surfaces. The spheres were then lyophilized for three days.

DPD Model Details: The DPD model was adapted from past studies of a similar nature.[16,17] In this model, three forces were applied to each particle (representing the repeating units of the polymer chain) at each time step—a conservative, a random, and a dissipative force. The form and value of all three of these forces are shown in the Supporting Information, as has been done in prior works.[12,17,19] Star polymers were created by linking beads together with harmonic springs to a single polymer core bead. Systems were thermalized for 30 000 timesteps, and then run for five million steps to equilibrate. The amount of solvent was kept fixed at one million particles. Four different arm lengths were

run: N_{bead} = 10, 40, 80, or 120 beads per arm. All simulations were performed for 4, 8, and 16 arms. In addition, to verify the effect of the hydroxyl stabilizer, two nonhollow cases were tested separately: eight arms, N_{bead} = 120 at polymer concentrations of both 10% and 13%. The strength of the hydroxyl–solvent and hydroxyl–hydroxyl repulsion was decreased, thereby increasing the preference for the hydroxyls to aggregate at the polymer/solvent interface. In these cases, a hollow to nonhollow transition was triggered when hydroxyl's affinity to glycerol was increased, consistent with the hydroxyl doubling experimental results. Finally, to ensure reproducibility of the structures, three independent runs were conducted for 50 million time steps each using Blue Waters. These runs were also used to create the movies contained in the Supporting Information.

All simulations were performed using the DPD implementation in HOOMD-Blue, a free and open-source code developed and maintained at the University of Michigan (http://codeblue.umich.edu/hoomd-blue). Images of the droplets and movies were created using VMD, a free visualization package available online. More details about the simulation can be found in the Supporting Information.

Supporting Information

Supporting Information is available from the Wiley Online Library or from the author.

Acknowledgements

The authors gratefully acknowledge financial support from the NIH (NIDCR DE022327, DE015384, and NHLBI HL114038: PXM), DOD (W81XWH-12-2-0008: PXM), and NSF (DMR-1206575: PXM). The simulation work (R.L.M. and S.C.G.) was supported by the U.S. Army Research Office under Grant Award No. W911NF-10-1-0518. Computer resources were provided, in part, by the Blue Waters sustained-petascale computing project, which was supported by the National Science Foundation (Award Nos. OCI-0725070 and ACI-1238993) and the state of Illinois. Blue Waters is a joint effort of the University of Illinois at Urbana-Champaign and its National Center for Supercomputing Applications. R.L.M. is grateful to J. Glaser and J. Anderson for discussions regarding DPD simulations.

Received: March 19, 2015
Revised: April 17, 2015
Published online: May 26, 2015

[1] a) R. Langer, *Nature* **1998**, *392*, 5; b) C. Barbé, J. Bartlett, L. Kong, K. Finnie, H. Q. Lin, M. Larkin, S. Calleja, A. Bush, G. Calleja, *Adv. Mater.* **2004**, *16*, 1959; c) W. Zhao, H. Chen, Y. Li, A. Li, M. Lang, J. Shi, *Adv. Funct. Mater.* **2008**, *18*, 2780.
[2] a) B. Comiskey, J. D. Albert, H. Yoshizawa, J. Jacobson, *Nature* **1998**, *394*, 253; b) A. N. Shipway, E. Katz, I. Willner, *Chem. Phys. Chem.* **2000**, *1*, 18.
[3] Y. Xia, B. Gates, Y. Yin, Y. Lu, *Adv. Mater.* **2000**, *12*, 693.
[4] Y. S. Xia, T. D. Nguyen, M. Yang, B. Lee, A. Santos, P. Podsiadlo, Z. Y. Tang, S. C. Glotzer, N. A. Kotov, *Nat. Nanotechnol.* **2011**, *6*, 580.
[5] J. I. Park, T. D. Nguyen, G. D. Silveira, J. H. Bahng, S. Srivastava, G. P. Zhao, K. Sun, P. J. Zhang, S. C. Glotzer, N. A. Kotov, *Nat. Commun.* **2014**, *5*, 3593.
[6] S. R. White, N. R. Sottos, P. H. Geubelle, J. S. Moore, M. R. Kessler, S. R. Sriram, E. N. Brown, S. Viswanathan, *Nature* **2001**, *409*, 794.
[7] a) F. Svec, J. M. Frechet, *Science* **1996**, *273*, 205; b) S. W. Kim, M. Kim, W. Y. Lee, T. Hyeon, *J. Am. Chem. Soc.* **2002**, *124*, 7642; c) J. Lee, J. C. Park, H. Song, *Adv. Mater.* **2008**, *20*, 1523.
[8] a) P. X. Ma, *Mater. Today* **2004**, *7*, 30; b)L. R. Madden, D. J. Mortisen, E. M. Sussman, S. K. Dupras, J. A. Fugate, J. L. Cuy, K. D. Hauch, M. A. Laflamme, C. E. Murry, B. D. Ratner, *Proc. Natl. Acad. Sci. USA* **2010**, *107*, 15211; c) S. J. Hollister, *Nat. Mater.* **2005**, *4*, 518.
[9] a) Z. Zhang, J. Hu, P. X. Ma, *Adv. Drug Delivery Rev.* **2012**, *64*, 1129; b) S. Zhang, *Nat. Biotechnol.* **2003**, *21*, 1171; c) J. D. Hartgerink, E. Beniash, S. I. Stupp, *Science* **2001**, *294*, 1684; d) H. W. Kim, J. H. Song, H. E. Kim, *Adv. Funct. Mater.* **2005**, *15*, 1988.
[10] X. Liu, X. Jin, P. X. Ma, *Nat. Mater.* **2011**, *10*, 398.
[11] Y. Zhao, X. Shuai, C. Chen, F. Xi, *Chem. Mater.* **2003**, *15*, 2836.
[12] P. X. Ma, R. Zhang, *J. Biomed. Mater. Res.* **1999**, *46*, 60.
[13] R. L. Marson, C. L. Phillips, J. A. Anderson, S. C. Glotzer, *Nano Lett.* **2014**, *14*, 2071.
[14] P. J. Flory, *J. Chem. Phys.* **1941**, *9*, 660.
[15] W. Zhang, S. Zheng, *Polym. Bull.* **2007**, *58*, 767.
[16] R. D. Groot, P. B. Warren, *J. Chem. Phys.* **1997**, *107*, 4423.
[17] C. L. Phillips, J. A. Anderson, S. C. Glotzer, *J. Comput. Phys.* **2011**, *230*, 7191.
[18] J. A. Anderson, C. D. Lorenz, A. Travesset, *J. Comput. Phys.* **2008**, *227*, 5342.
[19] T. D. N. Jens Glaser, J. A. Anderson, P. Lui, F. Spiga, J. A. Millan, D. C. Morse, S. C. Glotzer, *Comput. Phys. Commun.* **2014**, *192*, 97.